





Article

Development and Performance Analysis of a Low-Cost Redox Flow Battery

Nayeem Md. Lutful Huq^{1,2}, Islam Mohammed Mahbubul^{1,*}, Gazi Lotif³, Md. Rabbul Ashrafi² and Miah Himan¹

¹ Institute of Energy Engineering, Dhaka University of Engineering & Technology, Gazipur (DUET), Gazipur 1707, Bangladesh; lutful@duet.ac.bd (N.M.L.H.); 21273012@student.duet.ac.bd (M.H.)

² Department of Mechanical Engineering, Dhaka University of Engineering & Technology, Gazipur (DUET), Gazipur 1707, Bangladesh; 193006@student.duet.ac.bd

³ Department of Chemical Engineering, Dhaka University of Engineering & Technology, Gazipur (DUET), Gazipur 1707, Bangladesh; 198025@student.duet.ac.bd

* Correspondence: mahbubul@duet.ac.bd

Abstract: Redox Flow Batteries (RFBs) offer a promising solution for energy storage due to their scalability and long lifespan, making them particularly attractive for integrating renewable energy sources with fluctuating power output. This study investigates the performance of a prototype Zinc-Chlorine Flow Battery (ZCFB) designed for low-cost and readily available electrolytes. The ZCFB utilizes a saltwater electrolyte containing ZnCl₂ and NaCl, paired with a mineral spirits catholyte. The electrolyte consists of a 4 M ZnCl₂ and a 2 M NaCl solution, both with a pH of 4.55. The anode was a zinc metal electrode, while the cathode comprised a porous carbon electrode on a titanium grid current collector. The cell volume was approximately 4.0 mL, with separate reservoirs for the NaCl/H₂O and mineral spirits electrolytes. Experiments were conducted under constant current conditions, with a 0.2 A charging current and a 5 mA discharge current chosen for optimal cell voltage. The study analyzed the relationship between voltage, current, power, and capacity during both charging and discharging cycles. Results from multiple charge/discharge cycles found that the current density of the battery is around 62.658 mA/cm² with an energy capacity average of 1.2 Wh. These findings can contribute to the development of more efficient and practical ZCFBs, particularly for applications requiring low-cost and readily available electrolytes.

Keywords: renewable energy; membrane less redox flow battery; electrochemical energy storage; zinc-chlorine flow battery; electrolyte flow rate; large scale energy storage



Citation: Huq, N.M.L.; Mohammed Mahbubul, I.; Lotif, G.; Ashrafi, M.R.; Himan, M. Development and Performance Analysis of a Low-Cost Redox Flow Battery. *Processes* **2024**, *12*, 1461. <https://doi.org/10.3390/pr12071461>

Academic Editor: Qunjie Xu

Received: 4 May 2024

Revised: 6 July 2024

Accepted: 8 July 2024

Published: 12 July 2024



Copyright: © 2024 by the authors. Licensee MDPI, Basel, Switzerland. This article is an open access article distributed under the terms and conditions of the Creative Commons Attribution (CC BY) license (<https://creativecommons.org/licenses/by/4.0/>).

1. Introduction

Energy is one of the most important human needs for socioeconomic development. In the 21st century, addressing energy concerns is paramount due to depleting fossil fuels and environmental issues [1]. As fossil fuels become scarcer, alternative energy sources like wind and solar power are becoming more and more popular. Increased carbon emissions as a result of economic and technical expansion and population growth are what causes climate change and global warming [2,3]. Renewables like solar and wind are leading the charge against climate change and resource depletion. However, their dependence on the weather makes them unreliable. Nevertheless, solar and wind power are fundamentally remittent sources of energy with continuous and uncontrolled power output. It is challenging to implement the electricity generated from renewable sources properly into the existing power system [4].

Energy storage helps integrate renewable energy sources (RES) and distributed generation onto the grid. While RES reduces reliance on fossil fuels, their intermittent nature can compromise power quality and stability. Storage systems address this by offering backup power and smoothing out fluctuations, boosting energy independence for consumers [5].

Apart from the variable supply of renewable energy, storage plays an essential part in electrical power and voltage stabilizing [6]. For this reason, a variety of technologies are being developed, including some latest technologies like lithium-ion batteries, sodium sulfur batteries, vanadium redox flow batteries, super-capacitors, and superconducting magnetic energy [7].

Energy storage has become crucial for the modern grid due to the growing need for short-term power boosts. These systems act as power sources or perform functions like smoothing power fluctuations and improving overall grid stability [8]. Energy storage plays a crucial role in this transition, offering a bridge to cleaner and more efficient energy usage. From ancient methods like firewood to modern innovations, energy storage has evolved significantly. As global energy demand surges, efficient and adaptable energy storage solutions are vital for sustainable energy utilization across industries. Efficient energy storage revolutionizes the power industry by enabling widespread use of renewable sources like wind and solar. It enhances system reliability and stabilizes power dynamics as well as contributes to reducing harmful emissions. By leveling peak loads and improving efficiency, it lowers electricity costs. Moreover, it defers infrastructure upgrades, reduces transmission losses, and promotes distributed generation.

The electrochemical storage system (ECSS) consists of various types of batteries, which store electrical energy in the form of chemical energy [9]. Rechargeable batteries are an effective way to store energy. Lithium-ion, nickel-metal hydride (Ni-MH), lead acid, redox flow, and sodium-sulfur (Na-S), sodium-ion batteries are among the options [10,11]. Rechargeable aqueous aluminum ion electrochemistry offers high energy density, environmental friendliness, safety, and abundant resources, making it an ideal alternative energy storage system [12]. A novel aluminum-graphite dual-ion battery (AGDIB) in an ethyl-methyl carbonate (EMC) electrolyte is extremely reversible and energy-dense. In addition to offering a wide voltage window for a full battery, calcium-ion batteries (CIBs) are attractive choices for energy storage because Ca^{2+} has a low polarization and reduction potential that is comparable to Li^{+} 's [13,14]. NiS_2/NG , with its strong connection between conductive and active components, offers excellent structural integrity, high conductivity, and robust polysulfide adsorption capacity, ensuring quick reaction kinetics and energetically stable performance [15,16].

Battery storage systems are a promising solution, offering fast response, consistent power, and location flexibility. A critical challenge is finding the optimal battery size to balance the benefits (improved grid performance) with the added cost [17–19]. A Battery Energy Storage System (BESS) combines batteries with a control system and infrastructure. Batteries, evolving constantly, convert chemical energy into electricity through stacked cells connected for desired voltage and current. BESS design typically ties energy storage capacity to power output. Key factors include efficiency, lifespan, operating temperature, and discharge depth. Battery technology is advancing, with deep cycle batteries, like those in electric vehicles, commonly used in power systems, offering energy capacities of 17 to 40 MWh and efficiencies of 70–80% [20]. BESS offers quick, reliable power with environmental benefits and flexible placement [21]. Recent research interest in batteries has been driven by the diverse possibilities offered by different battery chemistries and cell designs, leading to a wide range of energy and power densities achievable.

A flow battery is an enhanced aqueous electrolytic battery that combines traditional fuel cells with batteries. The flow battery design is occasionally known as regenerative fuel cells or redox flow systems [10,22]. Flow batteries differ from traditional batteries by storing electrolytes in separate tanks and pumping them through electrode compartments, known as stacks, comprising multiple cells [23]. Flow batteries stand out for their ease of scalability. Unlike conventional batteries, adding more electrolytes or raising their concentration directly improves energy storage. Power is increased simply by adding cells to the stack. Because of the independence of power and energy capacity, a single system may be adjusted to meet different needs by modifying these components, making flow batteries very flexible for a wide range of applications [24,25]. They commonly utilize

two sets of electrolytes, with one passing by the positive electrode and the other by the negative electrode, each pumped through distinct loops. Within the cells, an ion-conducting membrane or micro-porous separator divides these electrolytes [23]. Unlike secondary batteries, one or more electro-active species dissolve in the electrolyte and store energy. This energy passes through the power core, which converts chemical energy into electricity. Additional electrolyte is kept in exterior tanks and pumped into the reactor [9,26]. Flow batteries are categorized into two types based on their electro-active components: redox flow batteries and hybrid flow batteries [27]. Challenges include resource constraints, safety concerns, and competition with established chemistries. Solutions involve developing sustainable, cost-effective electrolytes while maintaining performance standards [28,29]. Flow batteries face barriers such as overcharge-resistant electrodes, membrane degradation, electrolyte stability, and optimization challenges that need addressing for full economic potential in mobile and grid-scale systems [30]. Optimizing electrolyte flow rates will enhance energy efficiency by reducing energy pumping needs [30–33].

Hybrid flow batteries utilizing zinc present a compelling solution for medium to large-scale energy storage, boasting cost-effectiveness, favorable cell voltage, and enhanced energy density. Notably, several of these systems have progressed to commercialization, representing a significant advancement in flow battery technology. In these zinc-based configurations, the negative electrode reaction involves zinc electrode position within flowing fluids, paired with diverse organic or inorganic positive active species in solid, liquid, or gaseous states. Customized cell designs further optimize these processes for specific operational requirements [34]. Zinc-bromine batteries (ZBBs) are popular for distributed energy storage owing to their high theoretical energy density and cost-effectiveness.

The growing demand for renewable energy is driving the development of cost-effective energy storage technologies, such as redox flow batteries (RFBs). RFBs are the most common type of flow battery, containing electroactive chemicals in a liquid electrolyte. They create electricity through oxidation and reduction reactions and come in various electroactive materials like vanadium, vanadium-polyhalide, bromine-polysulphide, iron-chromium, and hydrogen-bromium [35]. RFBs have a novel design that includes a stack cell, energy storage tanks, and a flow mechanism. These batteries use active species dissolved in liquid electrolytes, which are stored separately from the electrodes. The catholyte and anolyte fluids circulate through the cells via a pump, allowing chemical energy to be converted into electrical energy [36]. RFBs are versatile flow batteries that can independently scale energy and power, making them suitable for various applications. Their unique design allows for separate storage for liquid electrolytes and electrochemical cells, enhancing their flexibility. Recent advancements in RFB technology show promise, offering design flexibility, improved safety, and high power density without the limitations of solid active materials [37].

Early redox flow battery research focused on using metal ions paired with halogen ions, particularly bromine and iodine. These halogens were chosen because their electron transfer properties (redox potentials) fall within a suitable range for water electrolysis, making them compatible with the battery system. Recent advancements in aqueous RFBs have seen a diversification of redox couples, going beyond halogens [36]. An electrochemical oxidation-reduction reaction converts the chemical energy in active materials into electrical energy [38]. The anode and cathode, two electrodes with opposing charges, make up a battery cell. These electrodes are submerged in an electrolyte, which might be viscous, liquid, or solid [27]. A small membrane separates electrolytes, allowing only a limited number of ions to pass through, facilitating oxidation and reduction events within a reactor, thereby generating energy [39].

Researchers are improving RFBs for large-scale energy storage by addressing challenges like storing large volumes of electrolyte solutions and their high costs. They are also conducting real-world tests and developing cost-optimizing models to make RFBs a strong contender in the future [37]. Currently, different types of vanadium redox flow batteries (VRFB) are considered promising and economically feasible flow batteries for storing inter-

mittent renewable energy since they use the same element for both anolyte and catholyte. VRFBs, a low parasitic loss, high-efficiency battery with a life cycle of over 10,000 cycles and 90% efficiency at low loads, are a viable option for stationary energy storage. These batteries maintain a constant voltage under all conditions and can be quickly recharged by refilling the electrolyte. VRFB stores energy using vanadium redox couples, a common electrolyte dissolved in sulfuric acid, and a polymer membrane blocking H_2SO_4^- ions passage during charging and discharging [9,26]. Despite several demonstrations, VRFB stacks still encounter obstacles in the commercialization process because of their high cost, especially the membrane component, which makes up about 41% of the total cost [40]. VRFB electrode development has seen significant progress through the deposition of various metal oxides (MnO_2 , Mn_3O_4 , PbO_2 , WO_3 , etc.) onto carbon felt via a hydrothermal process. This approach has resulted in improved performance metrics, such as increased peak currents, decreased cyclic voltammetry peak separation, and lower charge transfer resistance. These findings suggest enhanced electrocatalytic activity and faster reaction kinetics. Positive electrodes appear to benefit the most, with some studies reporting stable energy efficiency across multiple charge/discharge cycles [41]. During the charging and discharging procedures, current is applied or withdrawn using current collectors in RFBs. In order to electrochemically convert $\text{ZnCl}_2 + \text{NaCl}$ ions, current collectors receive and transmit current from an external power source to the electrodes during charging. The current collector plates, which are employed by external load resistance, receive the current produced by electrochemical processes during discharging. Therefore, the system's charging or discharging mode determines the direction of the current flow. Good electrical conductivity and non-corrosiveness in an acidic environment are requirements for the materials used in RFB current collectors. Carbon/Graphite [42], Au, Cu [43], Pt, or Ti [44] are common materials for current collectors.

Zinc-cerium redox flow batteries (ZCBs) are emerging as a highly promising technology, offering the potential to store large amounts of energy cost-effectively and efficiently. This is due to their possessing the highest thermodynamic open-circuit cell voltage among currently researched aqueous redox flow batteries. The ZCB utilizes Zn/Zn^{2+} and $\text{Ce}^{3+}/\text{Ce}^{4+}$ redox couples, achieving a maximum theoretical cell voltage of 2.50 V, which surpasses the typical 1.26 V found in all-vanadium redox flow batteries. This heightened cell voltage, particularly under specific electrolyte concentrations, can result in increased cell capacity and power [45].

Polysulfide-polybromide (PSB) batteries are redox flow batteries that use sulfur as an active ingredient and bromine as a main component. When combined with sulfide and bromide salts, they produce complexes like polysulfide and polybromide, which are soluble in aqueous solutions [46,47]. Sulfur has a large theoretical capacity, is non-toxic, and is inexpensive. The aqueous PSB battery arrangement uses a Na_2S anolyte and a NaBr catholyte, both abundant and inexpensive [36].

Commercial redox flow batteries currently face a significant limitation in their energy density, primarily due to the restricted solubility of electroactive materials in the electrolyte. A proposed solution involves utilizing solid electroactive materials instead of those that dissolve, potentially enhancing energy density while reducing costs and expanding application possibilities. Traditional RFBs typically employ porous carbon electrodes to increase surface area and improve battery performance [48]. Redox flow batteries can improve energy density by adding more solid particles to the electrolyte. However, this increases pressure, requires expensive separators, and reduces efficiency. There is a need for a balancing act between density and performance [48].

Reducing capital and cycle life costs is vital for energy storage adoption. The research aims to replace expensive ionic exchange membranes in vanadium redox batteries. Skyllas-Kazacos et al. [49] introduced a perfluorinated membrane substrate costing one-third less than Nafion, making it suitable for various applications. Developing new membrane materials for energy storage must meet various requirements beyond cost, including high conductivity, low vanadium ion permeability, chemical stability, oxidation resistance, and

fouling resistance. Water transfer behavior is crucial, particularly in VRFBs with Nafion membranes, which swell excessively and lead to pore opening and water transfer issues during cycling [50]. Nafion membranes offer stability in electrolytes but are costly, so alternative anion exchange membranes are used in VRB demonstration systems. These membranes, while cheaper, require high-purity vanadium electrolytes, increasing costs. Developing inexpensive, chemically stable membranes resistant to electrolyte impurities could lower stack costs and enable the use of lower-purity vanadium oxide, reducing overall system costs.

Several research gaps need to be addressed for the successful implementation of RFBs.

- Identification of suitable, low-cost, and sustainable electrode materials: existing RFBs often rely on expensive or environmentally concerning electrode materials like vanadium or cobalt, which are expensive and not readily available. Identifying abundant, low-cost, and environment-friendly alternatives suitable for Bangladesh's context is crucial.
- Optimizing performance of membrane-less saltwater RFBs: membrane-less RFBs offer a simpler design at a lower cost, but they face challenges due to electrolyte crossover. Research is needed to optimize electrode design, electrolyte composition, and flow rates to minimize crossover while maintaining good RFB performance.
- Saltwater electrolytes can introduce corrosion issues and degradation mechanisms not observed in traditional aqueous electrolytes. Research is needed to evaluate the long-term durability of electrode materials and cell components in saltwater environments.
- Techno-economic assessment: while focusing on low-cost materials, a techno-economic assessment is necessary to evaluate the overall economic feasibility of implementing these RFBs. This should consider factors like manufacturing costs, required energy storage capacity, and grid integration costs.

By addressing these research gaps, the study aims to develop an optimized redox flow battery design using the most available materials to reduce the cost of energy storage systems and to investigate the performance and durability of low-cost and sustainable redox flow batteries for renewable energy integration to promote sustainable energy development.

2. Materials and Methods

2.1. Materials

In this study, Ti material was used for current collectors. A saltwater electrolyte containing a 4 M ZnCl_2 and a 2 M NaCl solution paired with a mineral spirits catholyte was utilized. For this purpose, ZnCl_2 and NaCl salts were purchased from Merck, Göttingen, Germany. The mineral spirit was purchased from the local market. The physiochemical information of zinc chloride was a pH value of 5, density of 2.93 g/cm^3 , and solubility of 851 g/L. It was stored under $30 \text{ }^\circ\text{C} \pm 2 \text{ }^\circ\text{C}$. Similarly, sodium chloride with pH 7 has a density of 2.17 g/cm^3 and solubility 358 g/L. Then, the solution was prepared in the lab. To make 1 L of the 4 M ZnCl_2 solution, 545.12 g of ZnCl_2 powder and 116.88 g of NaCl powder of the 2 M NaCl solution were dissolved in distilled water. When these two solutions are combined, the resulting mixture has a measured pH of 4.55. The prototype utilizes a zinc metal electrode as the anode, with a silver (Ag) reference electrode. A porous carbon electrode serves as the cathode, with a current collector made of a titanium grid positioned on the cathode side. Mineral spirits, with a total volume of 800 mL, are employed as the storage medium. The tube containing the mineral spirits and the porous carbon working electrode has an inner diameter of 2.54 mm. The working electrode itself has a thickness of 2.1 mm, while the distance separating the working and counter electrodes is 3.0 mm. The counter electrode has a thickness of 0.8 mm. The cell has a height of 4.0 cm and an approximate volume capacity of 4.0 mL. The total volumes of the mineral spirits reservoir and the NaCl/ H_2O reservoir are 4.1 mL and 80 mL, respectively. The flow rates of the NaCl/ H_2O solution (Q_{aq}) and the mineral spirits (Q_{org}) are measured at 0.0333 mL/s and 0.0033 mL/s, respectively.

2.2. Equipment

A brief information on the equipment used in this study is listed in Table 1.

Table 1. List of the equipment used in this research.

Equipment	Manufacturer	Model	City	Country	Purpose	Accuracy
Semi-Micro Balance	Sartorius Lab Instruments GmbH & Co. KG	QUINTIX 125D-1S	Göttingen	Germany	Weight measurement	±0.01 mg
High-Capacity Balance	Sartorius Lab Instruments GmbH & Co. KG	QUINTIX 5101-1S	Göttingen	Germany	Weight measurement	±100 mg
pH Meter	Lutron Electronic Enterprise Co. Ltd.	PH-208	Taipei	Taiwan	pH measurement	±(0.02pH + 2d)
Stirrer	Nanjing Ronghua Scientific Equipment Co. Ltd.	MS-H280-Pro	Nanjing	China	Electrode/Solution Preparation	±1 °C (<100 °C) ±1 °C (>100 °C)
3D Printer	Anycubic	I3 mega s	Shenzhen	China	Cell Structure preparation	--
Hot Box Oven	Gallenkamp	OHG097.XX2.5	Nottingham	England	Drying Positive Electrode	--
SEM Analyzer	Hitachi High-Tech	SU-1510	Tokyo	Japan	Morphology Analysis	--
Battery Tester	Chroma ATE Inc.	17208M-6-30 8 Channel Battery cell Tester	Taoyuan	Taiwan	Charge/Discharge measurement	±0.02% of F.S.

Pumps are the only moving device of the RFB, and they are linked to the battery's positive and negative sides. They provide the cell stack with electrolytes from the storage tanks. The best options to accomplish this on a large scale and in a laboratory setting, respectively, are centrifugal and peristaltic pumps. Pipes are constructed of PTFE, PVDF, PET polyester, or PVC for RFB [51]. In this experiment, two centrifugal pumps were used. The additional information about this pump are voltage range of 2.5–6v D.C. power of 0.4–1.5 watts, a head of 40–110 cm, and a flow of 80–120 L/h.

The morphology of a porous carbon positive electrode and the zinc plate negative electrode were characterized by a scanning electron microscope (SEM) (Hitachi SU1510, Tokyo, Japan) operating at 10 kV. With a beam energy range spanning from 300 eV to 30 keV, it boasts a resolution of 4 nm in variable pressure scanning electron microscope (VP-SEM) mode. Magnification of up to 5000× is achievable, and a special Quad-Bias function is incorporated to enhance the signal-to-noise ratio at lower beam energies.

2.3. Methodology

Every electrochemical device, where anodic and cathodic processes take place, is powered by its electrode. It facilitates the exchange of electrons during reactions in RFBs with electrolytes. While it offers ZnCl₂ and NaCl reaction sites, it does not directly take part in the electrochemical process itself. Because of the high porosity of the carbon electrodes, ZnCl₂ and NaCl ions may be electrochemically converted at homogeneous reaction sites. They have a three-dimensional network, are inexpensive and light, do not corrode when exposed to acids, and have a very high electronic conductivity. A kind of cross-sectional view of the internal configuration is shown in Figure 1.

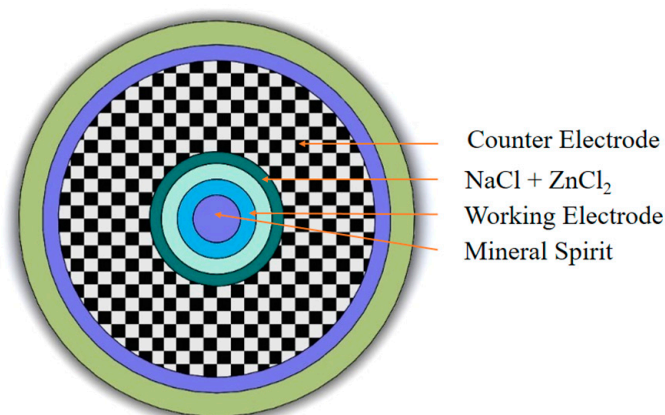


Figure 1. Internal Configuration of the System.

In this experiment, the single cell consists of a positive electrode, negative electrode, references electrode, and current collector. Porous carbon is good for the positive electrode. Polyvinyl alcohol (PVA) was used as an additive to bond the porous carbon to the titanium current collector. Positive electrodes were prepared using porous carbon, carbon black, PVA, and quantitatively distilled water. Then the mixture was stirred at 80 degrees Celsius and 1200 RPM for one and a half hours. Then it was heated for 14 h in a closed oven. Then the final cell setup was prepared as shown in Figure 2.

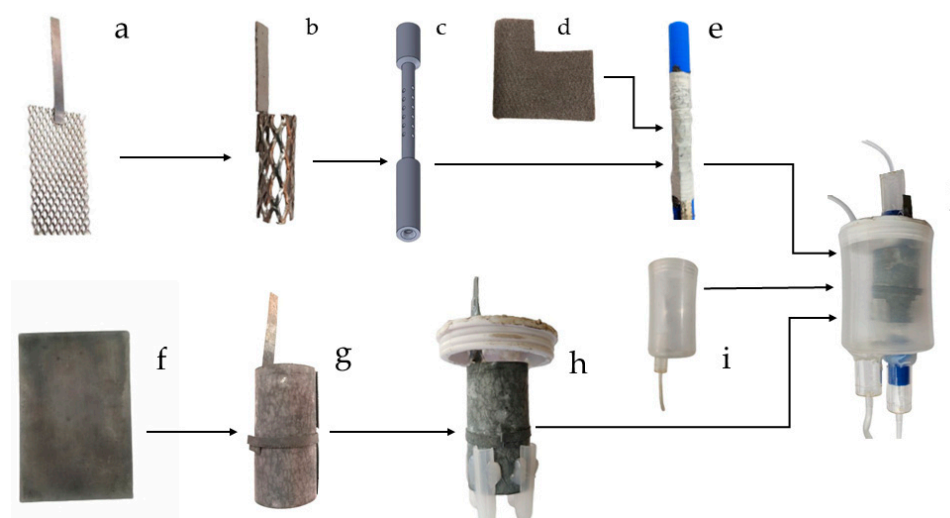


Figure 2. Preparation of cell assembly, (a) Titanium mesh, (b) Current collector, (c) 3D printed structure, (d) Porous carbon, (e) Positive electrode with a current collector and porous carbon, (f) Zinc plate, (g) Cylindrical shape of the zinc plate, (h) Negative electrode mounted with polypropylene structure, (i) Outer structure made of polypropylene, (j) Final cell.

The carbon materials were tested in a three-electrode cell setup consisting of porous carbon as the working electrode, titanium references electrode, and zinc plate counter electrode as shown in Figure 3. Precise measurements in electrochemistry rely on the three-electrode setup. The working electrode, typically glassy carbon, initiates reactions with specialized materials addressing specific needs. The reference electrode ensures accuracy by maintaining a stable redox couple. Non-aqueous environments commonly utilize the Ag/Ag⁺ electrode, while aqueous solutions might employ Saturated Calomel Electrodes or Ag/AgCl electrodes. The counter electrode mirrors, the opposite process of the working electrodes, usually made of platinum wires. Assembly involves fitting electrodes with O-rings into a glass cell and connecting the leads accordingly. For the non-aqueous Ag/Ag⁺ electrode, a silver wire in a Teflon housing is paired with a glass capillary containing a

Vycor tip. This capillary is then filled with reference electrode solution and nicely fitted. The concept of the three-electrode setup is originated by Hou et al. [52]. In-depth explanations of this topic are available in ref. [53].

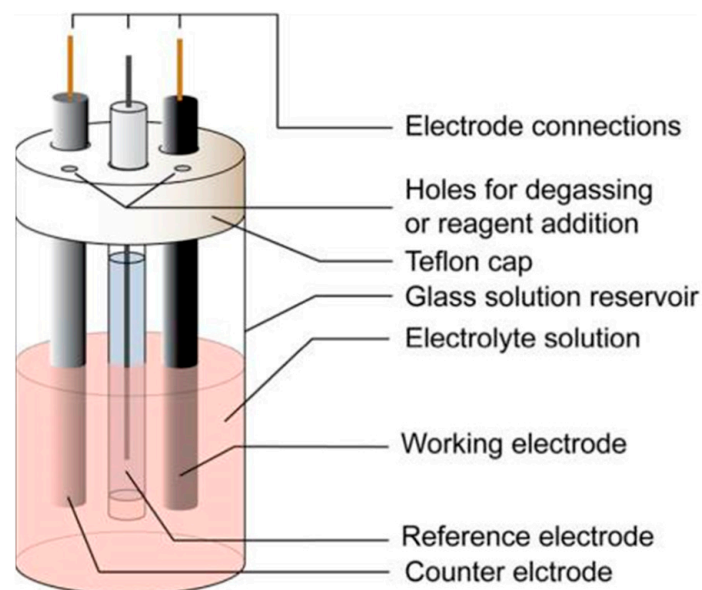
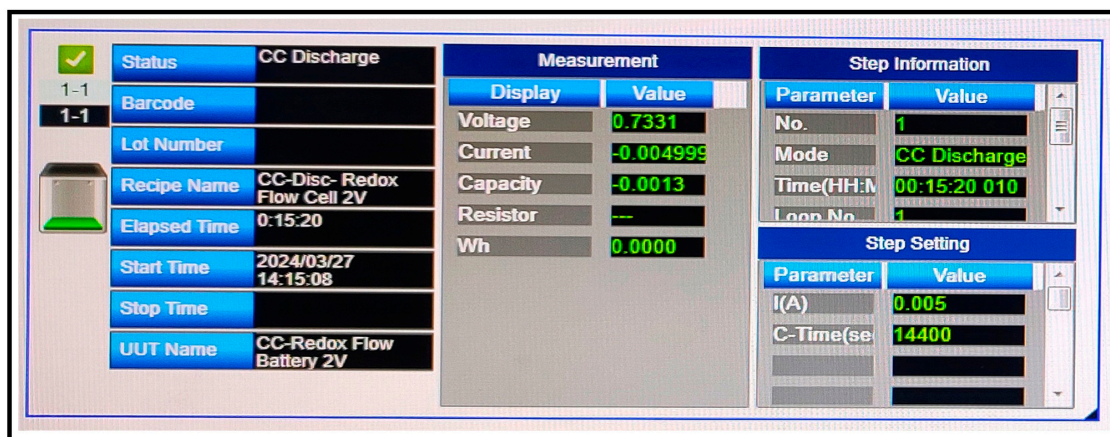


Figure 3. Three Electrode Configurations System {reprinted from [54], © 2017 American Chemical Society and Division of Chemical Education, Inc.}.

Figure 4 illustrates a schematic of the experimental setup for RFBs, which includes positive and negative electrolyte tanks, a single-cell active area of 10 cm^2 , two centrifugal pumps, a redox flow battery test station, and a computer. The tanks are filled with the appropriate electrolyte solutions, which are circulated throughout the cell via connecting pipelines and centrifugal pumps. The working and counter electrode clips link the cell to the test station, allowing current to be applied or withdrawn.

Battery performance was evaluated through a Chroma 17208M-6-30 programmable charge and discharge tester via a two-step process: hardware setup and software configuration. In the hardware setup, the tester is ensured to be correctly connected and powered, followed by the battery to be tested being connected to one of its channels, with proper polarity being ensured to prevent damage. Software configuration is achieved through the Chroma 17011 (Ver. 1.12) Battery Pro program, where the battery type is specified, and charging and discharging currents are then set within safe ranges. Voltage cut-offs for both charging and discharging cycles are defined based on the battery's datasheet. The test duration or number of cycles is then determined, and data logging is enabled to record voltage, current, and other relevant parameters for later analysis. After the battery is securely connected to the tester and the software parameters are set, the test is initiated. The software takes control, automatically cycling the battery through the charging and discharging phases.

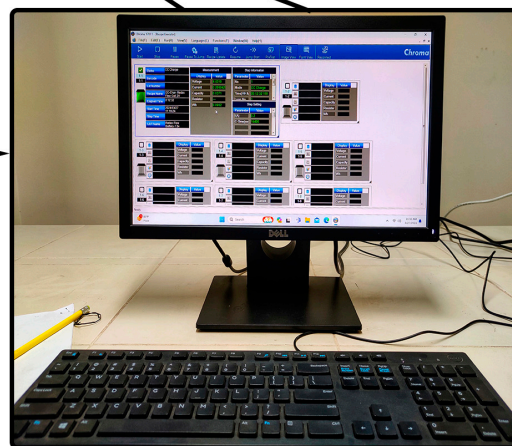
The charge test is initiated, during which controlled current and voltage are supplied by the tester until the battery reaches the desired charge level or cutoff voltage. Following this, switching to discharge mode allows current to be drawn from the battery at a controlled rate until it reaches the cutoff voltage or specified endpoint. Throughout the test, parameters like voltage, current, and capacity are monitored, ensuring they remain within safe limits. Once complete, the data collected by the tester is analyzed for any anomalies or deviations from expected performance, such as capacity loss or irregular charging/discharging behavior. The test results and observations are documented for further analysis. The loss of capacity during discharge compared to charge is expressed as a percentage.



Chroma 17208M-6-30



TCP/IP



Battery Cell Connector

Host Computer

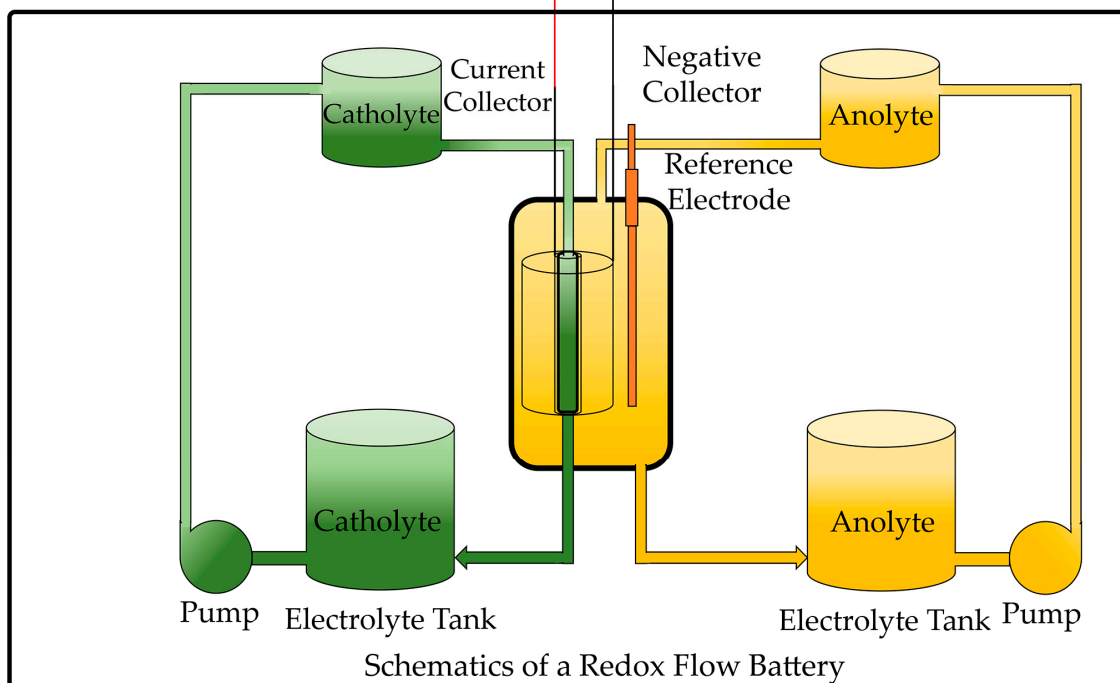


Figure 4. Experimental Setup.

3. Results and Discussion

3.1. Morphology Analysis

The SEM images of the porous carbon are shown in Figure 5. Figure 5a,b shows SEM images of the positive electrode morphologies. Figure 5a represents the untreated electrode, which shows some holes were created. The fibrous structures are densely packed, forming a network that likely contributes to the material's mechanical properties. Several small pores, approximately 10–20 μm in diameter, are visible throughout the image, suggesting potential sites for fluid infiltration. Figure 5b represents the electrode conditions after the test. Comparing Figure 5b with the untreated sample (Figure 5a), it is evident that the treatment process has significantly increased the porosity and altered the surface texture. Figure 5 shows that the porous carbon was successfully loaded with carbon sheets, enhancing the wettability of the electrode for its distinctive structure. The electrolyte flow's conductivity was improved by the presence of carbon sheets, diverse diffusion pathways were created, and the local flow velocity was increased. Some other literature showed SEM images of different types of carbon electrodes [55,56].

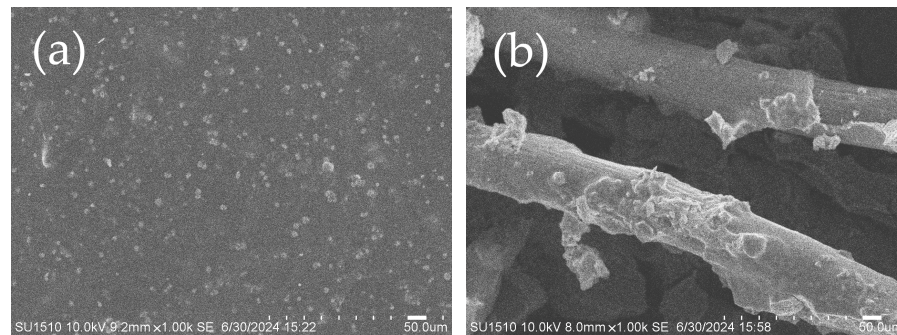


Figure 5. SEM images of the positive electrode (a) before and (b) after the electrodeposition treatment.

In this experiment, pure zinc was used as the negative electrode. The SEM images of the zinc plate were performed before and after electrodeposition at different magnification scales. Figure 6a–f shows the surface morphology of the zinc plate at three different scale bars representing 1 mm, 300 μm , and 500 μm . SEM analysis revealed significant differences before and after treatment. Figure 6a–c shows that the initial zinc plate was not smooth enough, whereas Figure 6d–f shows visible corrosion evident on the surface because of the treatment. Similar types of corrosion trends were observed in [57].

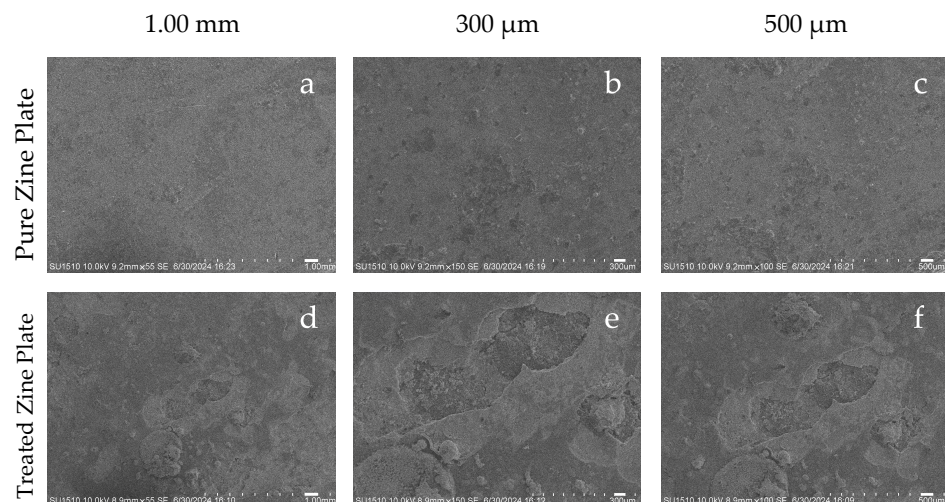
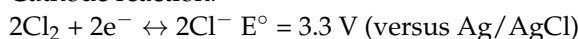


Figure 6. (a–c) morphologies of the negative electrode before electrodeposition, and (d–f) after electrodeposition.

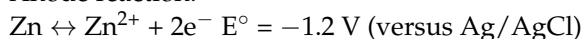
3.2. Charging/Discharging Analysis

In this study, an investigation was conducted to evaluate the Cl_2/Cl^- redox reaction within a $\text{ZnCl}_2\text{-NaCl}$ aqueous solution for application in a $\text{Zn}/\text{Cl}_2\text{-mineral spirits}$ flow battery. A concentric cell was utilized, featuring a working electrode comprised of $\text{RuO}_2\text{-TiO}_2$ coated carbon foam, a zinc counter electrode, and an Ag/AgCl reference electrode. This design deviates from traditional flow batteries by separating the $\text{Cl}_2\text{-mineral spirits}$ and $\text{ZnCl}_2\text{-NaCl}/\text{H}_2\text{O}$ streams, capitalizing on their immiscibility to eliminate the requirement for an ion-permeable membrane. During charging, Cl_2 is generated by oxidizing Cl^- ions within the $\text{RuO}_2\text{-TiO}_2$ coated carbon electrode. The reaction shows a constant potential at 3.3 V vs. Ag/AgCl . The Cl_2 is then stored in the mineral spirits. The $\text{Cl}_2\text{-mineral spirits}$ exhibit low and stable viscosity, even with increasing Cl_2 concentration, reducing pumping losses and maintaining consistent solution flow throughout the cell. When 6.0 mL mineral spirits were used, the maximum reversible capacity for Cl_2/Cl^- conversion was 600 mAh, rendering the capacity of 97 Ah/L for the $\text{Cl}_2\text{-mineral spirits}$. During discharge, the Cl_2 in mineral spirits was reduced to Cl^- in the working electrode and entered the $\text{ZnCl}_2\text{-NaCl}/\text{H}_2\text{O}$ [52].

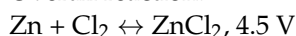
Cathode reaction:



Anode reaction:



Overall reaction:



While the overpotentials enhanced as the current density increased, the discharge capacities did not vary, which could be attributed to the large reaction surface area endowed by the wetting between the carbon electrode and $\text{Cl}_2\text{-mineral spirits}$. It is worth noting that polarizations for discharge are more significant than those for discharge. In the Chlorine Flow Battery (CFB), overpotentials are caused by redox reactions and concentration gradient [52]. Charging and discharging starting and ending times are shown in Table 2.

Table 2. Charge/Discharge data with time.

Charge/Discharge Number	Starting Time	Ending Time	Time Duration
Charge 01	13:30	14:20	50 min
Discharge 01	14:20	14:40	20 min
Charge 02	20:08	20:20	12 min
Discharge 02	20:30	22:30	120 min

The analysis of the cells charging and discharging behavior is presented in Figure 7. It expresses voltage, current, power, and capacity curves over time for charging and discharging. An increasing trend of voltage during charging is observed in Figure 7a. A decreasing trend of the voltage curve was observed during discharging (can be seen in Figure 7a). Again, the increasing voltages were observed during the second charging profile of Figure 7a. Also, a decrease in voltages is observed during the second discharging in Figure 7a. Figure 7e is brought here to compare the performance of Figure 7a (present study) with that of [58]. RFBs. Their performance during two charge-discharge cycles is illustrated in Figure 7a,e, revealing that the charging and discharging times were almost similar.

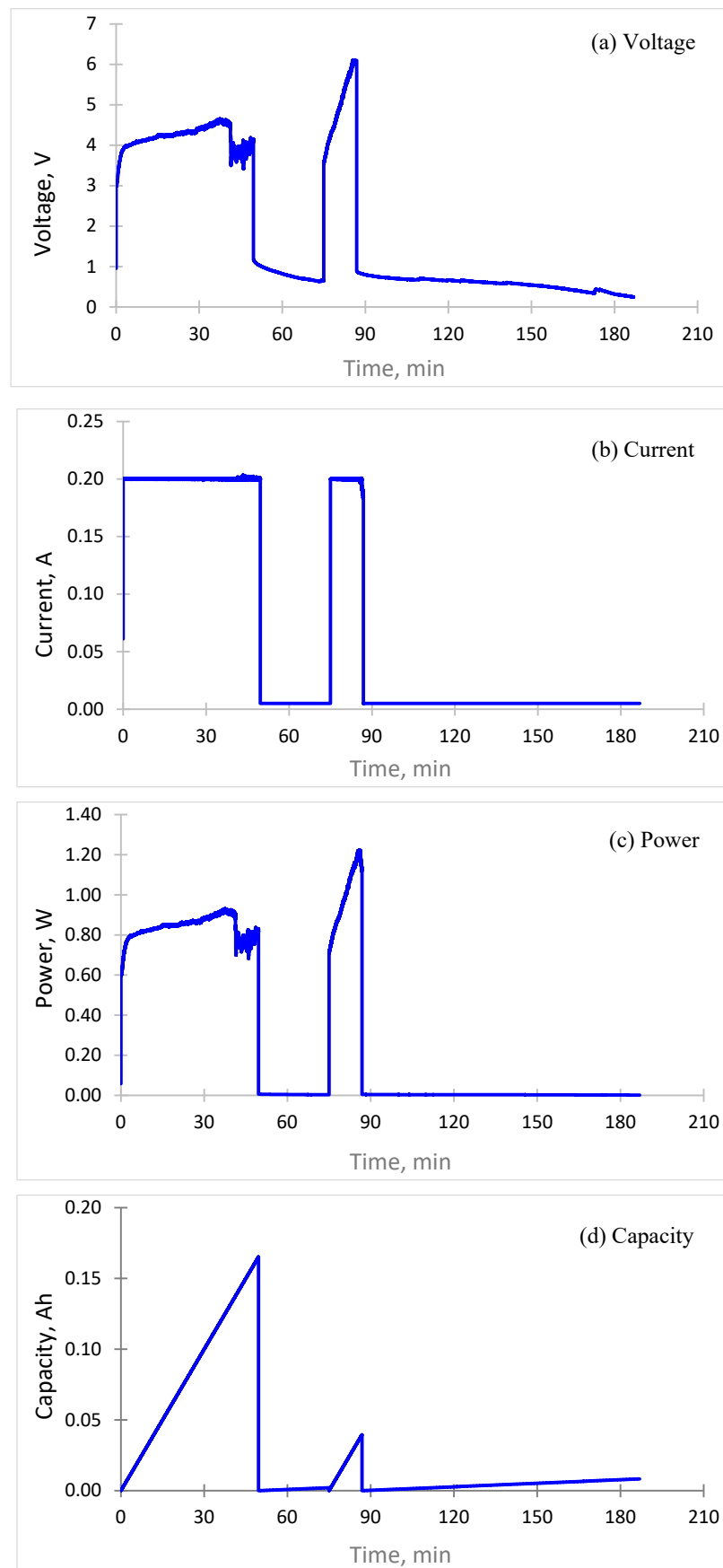


Figure 7. Cont.

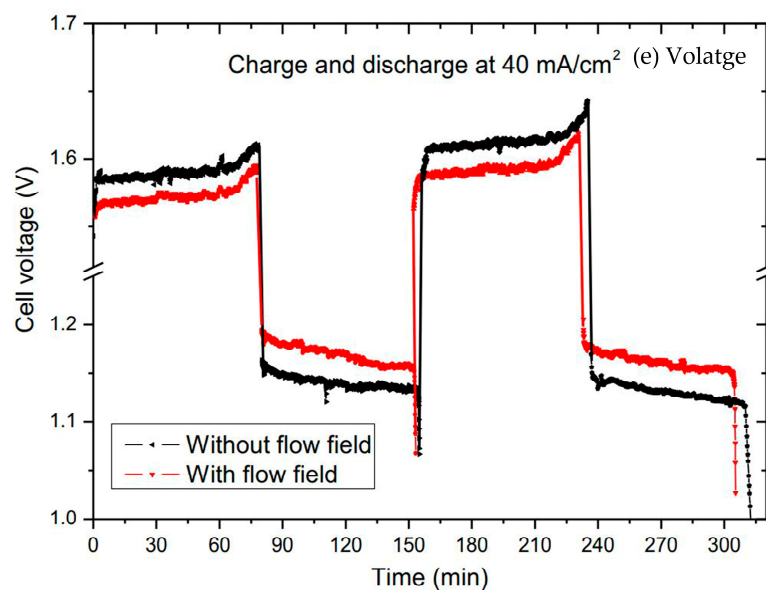


Figure 7. Charging-discharging profile, voltage (a), current (b), power (c), capacity (d), and voltage (e). {Figure 7e is reprinted from [58], Copyright (2014), with permission from Elsevier}.

Constant current conditions were employed throughout the experiments. A constant current of 0.2 A was used during the charging phases (Figure 7b), while discharge currents were meticulously chosen to ensure sufficient cell voltage remained. A discharge current of 5 mA was determined to be optimal for the system.

During charging No. 1, a voltage of up to 4.5 volts was achieved using the aforementioned 0.2 A charge current. Subsequently, the voltage was observed to be 0.6 volts after 20 min of discharging during the first step. Following the same procedure, charging No. 2 achieved a voltage of up to 6 volts while utilizing the 0.2 A charge current. Discharging No. 2 exhibited a voltage decrease to 0.246 volts after the second step. Figure 7c contains additional details such as power curves over time. The power curve reflects the combined voltage and current behaviors. Furthermore, capacity curves (Figure 7d) demonstrate energy storage and delivery trends. This analysis offers valuable insights into efficiency, energy storage capacity, and discharge rates for researchers.

In certain cases, electrolyte crossing can be reduced, allowing the use of outstanding cell components such as porous carbon and carbon black, as well as higher-grade binding materials and electrodes. Electrode optimization depends on electrode treatment that has a significant impact on reaction kinetics, which subsequently in consequence affects current density. Furthermore, screening more efficient materials for use as bipolar plates may result in decreased ohmic losses as well as reduced production costs because of the reduction in corrosion of titanium and zinc electrodes.

Figure 8a shows the performance of Zn/Cl₂-mineral spirits flow battery in the case of 1 L of the 4 M ZnCl₂ solution, and NaCl powder from the 2 M NaCl solution. The coulombic efficiency of a battery is determined as the percentage ratio between the (discharging capacity and charging capacity) × 100 [59]. Here, porous carbon are positive electrode and Zn is a negative electrode. From Figure 8a, the coulombic efficiency was found to be 21% when using ZnCl₂-NaCl as buffer solution by comparing with the coulombic efficiency (91%) as shown in Figure 8b [60]. Wang et al. [61] have shown comparatively better efficiency by implementing natural graphene (NG) and found an initial charge-discharge efficiency of just 28.6% and a high discharge capacity at a modest current density of 0.1 A. In addition, a clear charge-discharge initial Coulombic efficiency of 50.6% is observed by utilizing multilayer graphene (MLG) [61].

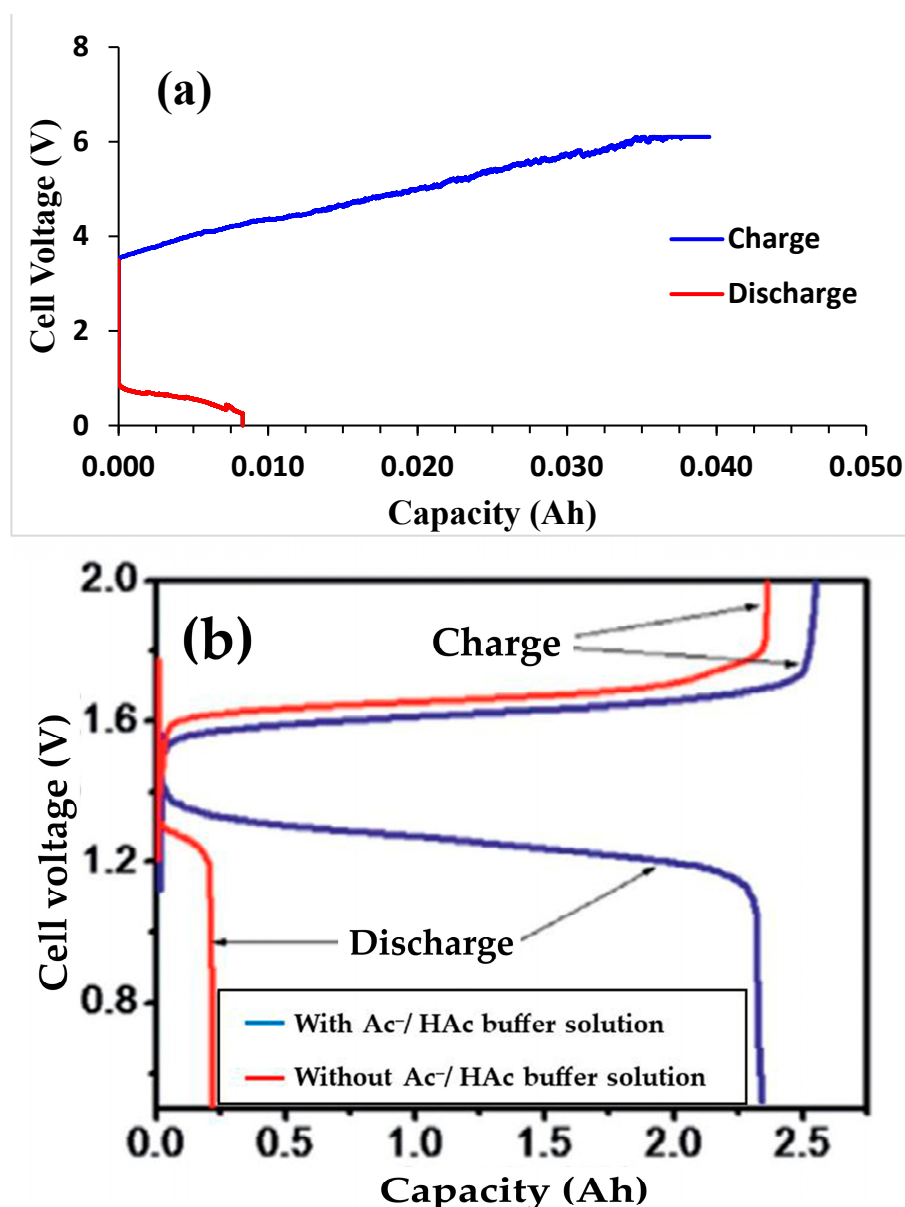


Figure 8. The RFB performance of (a) this study with ZnCl_2 - NaCl buffer solution and comparison with (b) {Adapted from [60], Copyright (2016), with permission from Science Press and Dalian Institute of Chemical Physics}.

4. Conclusions

- In this study, an investigation was conducted to evaluate the Cl_2/Cl^- redox reaction within a ZnCl_2 - NaCl aqueous solution for application in a Zn/Cl_2 -mineral spirits flow battery. A concentric cell was utilized, featuring a working electrode comprised of RuO_2 - TiO_2 coated carbon foam, a zinc counter electrode, and an Ag/AgCl reference electrode.
- A total of two cycles (charging-discharging) were analyzed because the developed battery cell was very small. It took about 50 min during the first time to complete the full charging, while discharging took only about 20 min. However, during the second charging, it took only 12 min to charge the cell and discharge continued until 120 min, which proved a promising aspect.
- During charging No. 1, a voltage of up to 4.5 volts was achieved using 0.2 A charge current. Subsequently, the voltage was observed to decrease by 0.6 volts over 20 min during discharging No. 1. Following the same procedure, charging No. 2 achieved a

voltage of up to 6 volts while utilizing the 0.2 A charge current. Discharging No. 2 exhibited a voltage decrease of 0.9 volts over a 120-min timeframe.

- To address RFB as an environmentally friendly technology, a specific emphasis must be placed on the use of harmful chemicals and materials, the prevention of electrolyte leakage in large-scale systems, and the use of renewable resources in the structural stack.
- This study did not identify RFB power connections with environmental compatibility and material sustainability.
- Furthermore, material degradation and corrosion in electrodes and other cells or stacks were not considered.
- One of the key elements in assessing a redox flow battery's overall efficiency is the assessment of pressure loss. Electrolyte flows through the channels, penetrates the porous electrode, and spreads over it for electrochemical reactions with the assistance of the pressure drop across the battery. Pumping expenses rise in response to pressure loss, which lowers system efficiency as a whole. In order to promote electrolyte flow, future studies are necessary to predict the pressure drop.
- The RFB's hybrid flow channel designs could be considered for use. Since the negative electrolyte's stated kinetics are quicker than those of the positive electrolyte; therefore, a thinner electrode can be employed on the negative side. As a consequence, channels could be utilized to minimize the pressure drop. It is also possible to change the flow directions from co-flow to counter-flow. These will assist in lowering the battery's volumetric density and maximizing its performance.
- In addition, inexpensive materials could be used to obtain higher power densities to minimize the cost per kilowatt. For example, by balancing the electrolyte motion, it is possible to achieve a reduced pressure drop, resulting in a smaller amount of pump losses and greater back-and-forth performance.
- An additional field for the researchers could be to further study how to scale up. In order to meet the criterion, future efforts might focus on utilizing these channels, which are intended for broader regions. As the channel is scaled up, its performance may vary, but it is still modifiable. Cell stacks can use these channels if the input and output ports are positioned correctly.

Author Contributions: Conceptualization, M.H.; Methodology, G.L., M.R.A. and M.H.; Formal analysis, I.M.M., G.L., M.R.A. and M.H.; Investigation, G.L. and M.R.A.; Writing—original draft, G.L., M.R.A. and M.H.; Writing—review & editing, I.M.M. and N.M.L.H.; Supervision, I.M.M.; Project administration, N.M.L.H.; Funding acquisition, N.M.L.H. All authors have read and agreed to the published version of the manuscript.

Funding: This research was funded by the University Grants Commission of Bangladesh through the Office of the Director (Research and Extension), DUET, Gazipur as a research project "Investigation of the Performance and Durability of Low-Cost and Sustainable Redox Flow Batteries for Renewable Energy Integration in Bangladesh" for the financial year 2023-24 and The APC was funded by MDPI as Author Voucher discount.

Data Availability Statement: The datasets presented in this article are not readily available because the data are part of an ongoing study. Requests to access the datasets should be directed to the corresponding author.

Acknowledgments: The authors would like to thank the laboratory staffs of the Institute of Energy Engineering and the Department of Mechanical Engineering of DUET. We are also thankful to the anonymous reviewers for their valuable comments to improve the quality of this manuscript.

Conflicts of Interest: The authors declare no conflict of interest.

References

1. Dincer, I. Energy and environmental impacts: Present and future perspectives. *Energy Sources* **1998**, *20*, 427–453. [\[CrossRef\]](#)
2. Wali, S.; Hannan, M.; Ker, P.J.; Rahman, S.; Le, K.N.; Begum, R.; Tiong, S.; Mahlia, T.I. Grid-connected lithium-ion battery energy storage system towards sustainable energy: A patent landscape analysis and technology updates. *J. Energy Storage* **2024**, *77*, 109986. [\[CrossRef\]](#)
3. Guo, Y.; Huang, J.; Feng, J.-K. Research progress in preparation of electrolyte for all-vanadium redox flow battery. *J. Ind. Eng. Chem.* **2023**, *118*, 33–43. [\[CrossRef\]](#)
4. Yuan, J.; Xue, Y.; Liu, L.; Zhang, J.; Xia, Y. Recent development of electrode materials in semi-solid lithium redox flow batteries. *J. Energy Storage* **2024**, *76*, 109574. [\[CrossRef\]](#)
5. Boicea, V.A. Energy storage technologies: The past and the present. *Proc. IEEE* **2014**, *102*, 1777–1794. [\[CrossRef\]](#)
6. Argyrou, M.C.; Christodoulides, P.; Kalogirou, S.A. Energy storage for electricity generation and related processes: Technologies appraisal and grid scale applications. *Renew. Sustain. Energy Rev.* **2018**, *94*, 804–821. [\[CrossRef\]](#)
7. Gamal, A.; Abdel-Basset, M.; Hezam, I.M.; Sallam, K.M.; Alshamrani, A.M.; Hameed, I.A. A computational sustainable approach for energy storage systems performance evaluation based on spherical-fuzzy MCDM with considering uncertainty. *Energy Rep.* **2024**, *11*, 1319–1341. [\[CrossRef\]](#)
8. Ribeiro, P.F.; Johnson, B.K.; Crow, M.L.; Arsoy, A.; Liu, Y. Energy storage systems for advanced power applications. *Proc. IEEE* **2001**, *89*, 1744–1756. [\[CrossRef\]](#)
9. Nadeem, F.; Hussain, S.S.; Tiwari, P.K.; Goswami, A.K.; Ustun, T.S. Comparative review of energy storage systems, their roles, and impacts on future power systems. *IEEE Access* **2018**, *7*, 4555–4585. [\[CrossRef\]](#)
10. Skyllas-Kazacos, M.; Chakrabarti, M.H.; Hajimolana, S.A.; Mjalli, F.S.; Saleem, M. Progress in Flow Battery Research and Development. *J. Electrochem. Soc.* **2011**, *158*, R55. [\[CrossRef\]](#)
11. Xue, S.; Shang, J.; Pu, X.; Cheng, H.; Zhang, L.; Wang, C.; Lee, C.-S.; Tang, Y. Dual anionic doping strategy towards synergistic optimization of Co₉S₈ for fast and durable sodium storage. *Energy Storage Mater.* **2023**, *55*, 33–41. [\[CrossRef\]](#)
12. Zheng, X.; Han, C.; Lee, C.-S.; Yao, W.; Zhi, C.; Tang, Y. Materials challenges for aluminum ion based aqueous energy storage devices: Progress and prospects. *Prog. Mater. Sci.* **2024**, *143*, 101253. [\[CrossRef\]](#)
13. Wang, M.; Jiang, C.; Zhang, S.; Song, X.; Tang, Y.; Cheng, H.-M. Reversible calcium alloying enables a practical room-temperature rechargeable calcium-ion battery with a high discharge voltage. *Nat. Chem.* **2018**, *10*, 667–672. [\[CrossRef\]](#) [\[PubMed\]](#)
14. Zhang, X.; Tang, Y.; Zhang, F.; Lee, C.-S. A novel aluminum–graphite dual-ion battery. *Adv. Energy Mater.* **2016**, *6*, 1502588. [\[CrossRef\]](#)
15. Luo, S.; Shang, J.; Xu, Y.; Cheng, H.; Zhang, L.; Tang, Y. Stabilizing NiS₂ on Conductive Component via Electrostatic Self-assembly and Covalent Bond Strategy for Promoting Sodium Storage. *Adv. Funct. Mater.* **2024**, 2403166. [\[CrossRef\]](#)
16. Yin, Y.; Yuan, Z.; Li, X. Rechargeable aqueous zinc–bromine batteries: An overview and future perspectives. *Phys. Chem. Chem. Phys.* **2021**, *23*, 26070–26084. [\[CrossRef\]](#)
17. Nehrir, M.; Wang, C.; Strunz, K.; Aki, H.; Ramakumar, R.; Bing, J.; Miao, Z.; Salameh, Z. A review of hybrid renewable/alternative energy systems for electric power generation: Configurations, control, and applications. *IEEE Trans. Sustain. Energy* **2011**, *2*, 392–403. [\[CrossRef\]](#)
18. Krishna, K.S.; Kumar, K.S. A review on hybrid renewable energy systems. *Renew. Sustain. Energy Rev.* **2015**, *52*, 907–916. [\[CrossRef\]](#)
19. Yang, Y.; Bremner, S.; Menictas, C.; Kay, M. Battery energy storage system size determination in renewable energy systems: A review. *Renew. Sustain. Energy Rev.* **2018**, *91*, 109–125. [\[CrossRef\]](#)
20. Divya, K.C.; Østergaard, J. Battery energy storage technology for power systems—An overview. *Electr. Power Syst. Res.* **2009**, *79*, 511–520. [\[CrossRef\]](#)
21. Hannan, M.A.; Wali, S.; Ker, P.J.; Abd Rahman, M.S.; Mansor, M.; Ramachandaramurthy, V.; Muttaqi, K.; Mahlia, T.M.I.; Dong, Z.Y. Battery energy-storage system: A review of technologies, optimization objectives, constraints, approaches, and outstanding issues. *J. Energy Storage* **2021**, *42*, 103023. [\[CrossRef\]](#)
22. Price, A. Technologies for energy storage—present and future: Flow batteries. In Proceedings of the 2000 Power Engineering Society Summer Meeting (Cat. No. 00CH37134), Seattle, WA, USA, 16–20 July 2000; pp. 1541–1545.
23. Fabjan, C.; Garche, J.; Harrer, B.; Jörisen, L.; Kolbeck, C.; Philippi, F.; Tomazic, G.; Wagner, F. The vanadium redox-battery: An efficient storage unit for photovoltaic systems. *Electrochim. Acta* **2001**, *47*, 825–831. [\[CrossRef\]](#)
24. Lota, G.; Graš-Ligočka, M.; Kolanowski, Ł.; Lota, K. Flow Batteries: Recent Advancement and Challenges. In *Handbook of Energy Materials*; Gupta, R., Ed.; Springer Nature: Singapore, 2022; pp. 1–21. [\[CrossRef\]](#)
25. Zhang, H.; Lu, W.; Li, X. Progress and Perspectives of Flow Battery Technologies. *Electrochem. Energy Rev.* **2019**, *2*, 492–506. [\[CrossRef\]](#)
26. Chen, H.; Cong, T.N.; Yang, W.; Tan, C.; Li, Y.; Ding, Y. Progress in electrical energy storage system: A critical review. *Prog. Nat. Sci.* **2009**, *19*, 291–312. [\[CrossRef\]](#)
27. Luo, X.; Wang, J.; Dooner, M.; Clarke, J. Overview of current development in electrical energy storage technologies and the application potential in power system operation. *Appl. Energy* **2015**, *137*, 511–536. [\[CrossRef\]](#)
28. Leung, P.; Shah, A.A.; Sanz, L.; Flox, C.; Morante, J.; Xu, Q.; Mohamed, M.; De León, C.P.; Walsh, F. Recent developments in organic redox flow batteries: A critical review. *J. Power Sources* **2017**, *360*, 243–283. [\[CrossRef\]](#)

29. Changyu, C.; Gaole, D.; Yuechen, G.; Peizhe, X.; Wei, H.; Shunan, F.; Xi, Z.; Yu, Z. Digitization of flow battery experimental process research and development. *Energy Mater.* **2024**, *4*, 400019.
30. Al-Fetlawi, H.; Shah, A.A.; Walsh, F. Non-isothermal modelling of the all-vanadium redox flow battery. *Electrochim. Acta* **2009**, *55*, 78–89. [[CrossRef](#)]
31. Al-Fetlawi, H.; Shah, A.A.; Walsh, F. Modelling the effects of oxygen evolution in the all-vanadium redox flow battery. *Electrochim. Acta* **2010**, *55*, 3192–3205. [[CrossRef](#)]
32. Shah, A.A.; Watt-Smith, M.; Walsh, F. A dynamic performance model for redox-flow batteries involving soluble species. *Electrochim. Acta* **2008**, *53*, 8087–8100. [[CrossRef](#)]
33. Shah, A.A.; Al-Fetlawi, H.; Walsh, F. Dynamic modelling of hydrogen evolution effects in the all-vanadium redox flow battery. *Electrochim. Acta* **2010**, *55*, 1125–1139. [[CrossRef](#)]
34. Khor, A.; Leung, P.; Mohamed, M.; Flox, C.; Xu, Q.; An, L.; Wills, R.; Morante, J.; Shah, A.A. Review of zinc-based hybrid flow batteries: From fundamentals to applications. *Mater. Today Energy* **2018**, *8*, 80–108. [[CrossRef](#)]
35. Nguyen, T.; Savinell, R.F. Flow batteries. *Electrochem. Soc. Interface* **2010**, *19*, 54. [[CrossRef](#)]
36. Pan, F.; Wang, Q. Redox species of redox flow batteries: A review. *Molecules* **2015**, *20*, 20499–20517. [[CrossRef](#)] [[PubMed](#)]
37. Chalamala, B.R.; Soundappan, T.; Fisher, G.R.; Anstey, M.R.; Viswanathan, V.V.; Perry, M.L. Redox flow batteries: An engineering perspective. *Proc. IEEE* **2014**, *102*, 976–999. [[CrossRef](#)]
38. Shao, Y.; Engelhard, M.; Lin, Y. Electrochemical investigation of polyhalide ion oxidation–reduction on carbon nanotube electrodes for redox flow batteries. *Electrochem. Commun.* **2009**, *11*, 2064–2067. [[CrossRef](#)]
39. Leung, P.; Li, X.; De León, C.P.; Berlouis, L.; Low, C.J.; Walsh, F.C. Progress in redox flow batteries, remaining challenges and their applications in energy storage. *RSC Adv.* **2012**, *2*, 10125–10156. [[CrossRef](#)]
40. Ding, C.; Zhang, H.; Li, X.; Liu, T.; Xing, F. Vanadium flow battery for energy storage: Prospects and challenges. *J. Phys. Chem. Lett.* **2013**, *4*, 1281–1294. [[CrossRef](#)] [[PubMed](#)]
41. Wu, Y.; Holze, R. Electrocatalysis at electrodes for vanadium redox flow batteries. *Batteries* **2018**, *4*, 47. [[CrossRef](#)]
42. Chakrabarti, M.; Brandon, N.; Hajimolana, S.; Tariq, F.; Yufit, V.; Hashim, M.; Hussain, M.; Low, C.; Aravind, P. Application of carbon materials in redox flow batteries. *J. Power Sources* **2014**, *253*, 150–166. [[CrossRef](#)]
43. Gandomi, Y.A.; Aaron, D.; Houser, J.; Daugherty, M.; Clement, J.; Pezeshki, A.; Ertugrul, T.; Moseley, D.; Mench, M. Critical review—Experimental diagnostics and material characterization techniques used on redox flow batteries. *J. Electrochem. Soc.* **2018**, *165*, A970. [[CrossRef](#)]
44. Arenas, L.F.; de León, C.P.; Walsh, F.C. Mass transport and active area of porous Pt/Ti electrodes for the Zn-Ce redox flow battery determined from limiting current measurements. *Electrochim. Acta* **2016**, *221*, 154–166. [[CrossRef](#)]
45. Xie, Z.; Liu, Q.; Chang, Z.; Zhang, X. The developments and challenges of cerium half-cell in zinc–cerium redox flow battery for energy storage. *Electrochim. Acta* **2013**, *90*, 695–704. [[CrossRef](#)]
46. Gross, M.M.; Manthiram, A. Long-life polysulfide–polyhalide batteries with a mediator-ion solid electrolyte. *ACS Appl. Energy Mater.* **2019**, *2*, 3445–3451. [[CrossRef](#)]
47. Zhou, H.; Zhang, H.; Zhao, P.; Yi, B. A comparative study of carbon felt and activated carbon based electrodes for sodium polysulfide/bromine redox flow battery. *Electrochim. Acta* **2006**, *51*, 6304–6312. [[CrossRef](#)]
48. Qi, Z.; Koenig, G.M. Flow battery systems with solid electroactive materials. *J. Vac. Sci. Technol. B* **2017**, *35*, 040801. [[CrossRef](#)]
49. Skyllas-Kazacos, M.; Kazacos, G.; Poon, G.; Verseema, H. Recent advances with UNSW vanadium-based redox flow batteries. *Int. J. Energy Res.* **2010**, *34*, 182–189. [[CrossRef](#)]
50. Sukkar, T.; Skyllas-Kazacos, M. Water transfer behaviour across cation exchange membranes in the vanadium redox battery. *J. Membr. Sci.* **2003**, *222*, 235–247. [[CrossRef](#)]
51. Gupta, A.; Allison, C.A.; Chaudhari, M.; Zalavadiya, P.; de Souza, F.M.; Gupta, R.K.; Dawsey, T. A Facile approach to recycling used facemasks for high-performance energy-storage devices. In *Specialty Polymers*; CRC Press: Boca Raton, FL, USA, 2023; pp. 427–443.
52. Hou, S.; Chen, L.; Fan, X.; Fan, X.; Ji, X.; Wang, B.; Cui, C.; Chen, J.; Yang, C.; Wang, W. High-energy and low-cost membrane-free chlorine flow battery. *Nat. Commun.* **2022**, *13*, 1281. [[CrossRef](#)]
53. Suzuki, H.; Hirakawa, T.; Sasaki, S.; Karube, I. An integrated three-electrode system with a micromachined liquid-junction Ag/AgCl reference electrode. *Anal. Chim. Acta* **1999**, *387*, 103–112. [[CrossRef](#)]
54. Elgrishi, N.; Rountree, K.J.; McCarthy, B.D.; Rountree, E.S.; Eisenhart, T.T.; Dempsey, J.L. A Practical Beginner’s Guide to Cyclic Voltammetry. *J. Chem. Educ.* **2018**, *95*, 197–206. [[CrossRef](#)]
55. Gao, Y.; Wang, H.; Ma, Q.; Wu, A.; Zhang, W.; Zhang, C.; Chen, Z.; Zeng, X.-X.; Wu, X.; Wu, Y. Carbon sheet-decorated graphite felt electrode with high catalytic activity for vanadium redox flow batteries. *Carbon* **2019**, *148*, 9–15. [[CrossRef](#)]
56. Zhang, H.; Sun, C.; Ge, M. Review of the Research Status of Cost-Effective Zinc–Iron Redox Flow Batteries. *Batteries* **2022**, *8*, 202. [[CrossRef](#)]
57. Yuan, Z.; Duan, Y.; Liu, T.; Zhang, H.; Li, X. Toward a Low-Cost Alkaline Zinc–Iron Flow Battery with a Polybenzimidazole Custom Membrane for Stationary Energy Storage. *iScience* **2018**, *3*, 40–49. [[CrossRef](#)] [[PubMed](#)]
58. Xu, Q.; Zhao, T.S.; Zhang, C. Performance of a vanadium redox flow battery with and without flow fields. *Electrochim. Acta* **2014**, *142*, 61–67. [[CrossRef](#)]

59. Wang, X.; Luo, Z.; Huang, J.; Chen, Z.; Xiang, T.; Feng, Z.; Wang, J.; Wang, S.; Ma, Y.; Yang, H.; et al. S/N-co-doped graphite nanosheets exfoliated via three-roll milling for high-performance sodium/potassium ion batteries. *J. Mater. Sci. Technol.* **2023**, *147*, 47–55. [[CrossRef](#)]
60. Xie, Z.; Su, Q.; Shi, A.; Yang, B.; Liu, B.; Chen, J.; Zhou, X.; Cai, D.; Yang, L. High performance of zinc-ferrum redox flow battery with Ac⁻/HAc buffer solution. *J. Energy Chem.* **2016**, *25*, 495–499. [[CrossRef](#)]
61. Wang, X.; Xia, Y.; Huang, J.; Su, Y.; Chen, Z.; Chen, L.; Wu, Z.; Feng, Z.; Yang, H.; Li, X. A facile strategy for large-scale production of 2D nanosheets exfoliated by three-roll milling. *J. Adv. Ceram.* **2024**, *13*, 11–18. [[CrossRef](#)]

Disclaimer/Publisher’s Note: The statements, opinions and data contained in all publications are solely those of the individual author(s) and contributor(s) and not of MDPI and/or the editor(s). MDPI and/or the editor(s) disclaim responsibility for any injury to people or property resulting from any ideas, methods, instructions or products referred to in the content.